Mechatronics 44 (2017) 14–23

Contents lists available at ScienceDirect

Mechatronics

journal homepage: www.elsevier.com/locate/mechatronics

Real time implementation of H-infinity and RST motion control of rotary traveling wave ultrasonic motor☆

M. Brahim*, I. Bahri, Y. Bernard

Group of Electrical Engineering of Paris (GeePs), University of Paris sud, 11 rue Joliot Curie 91192 Gif sur Yvette, France

ARTICLE INFO

Article history:
Received 19 September 2016
Revised 1 April 2017
Accepted 4 April 2017
Available online 15 April 2017

Keywords:
H-infinity
RST
Robustness
Piezoelectric motor
Motion control
Stability criteria

ABSTRACT

This paper deals with design, performances comparison and experimental validation of H-infinity (H_∞) and discrete time RST position controllers for a Traveling Wave Ultrasonic Motor (TWUM) which is dedicated to robotic applications. The proposed positioning system shows high precision levels of piezoelectric motor without additional hysteresis and dead zone compensation systems. Moreover, the perturbation rejection capability and the robustness to motor parameters variation are guaranteed. The synthesis procedure of robust H∞ and RST position controllers is detailed. The performances of the proposed controllers are validated by simulation and experimental results.

1. Introduction

Traveling Wave Ultrasonic Motor (TWUM) uses the reverse piezoelectric effect to generate motion. Ultrasonic Motors (USMs) consist of piezoelectric ceramics placed in the surface of a ring-shape elastic body (stator) and a rotor strongly pressed to it [1]. A flexural wave will be created at the stator surface when the ceramic is supplied with two phase shifted voltages at a frequency range close to the motor mechanical resonance frequency (f_r). This wave is able to move the rotor due to large friction produced by the contact mechanism. This friction is at the origin of the high holding torque without supply of USMs [2]. This feature makes the TWUM as an attractive solution for holding position of robotic arms in the case of off-power. With electromagnetic motors, the arm position is held by additional mechanical system. The high torque to mass ratio, fast response, high precision, non-magnetic proprieties, and high torque at low speed without gears have also made TWUMs an interesting choice for numerous applications; including Magnetic Resonance Imaging (MRI) surgical robots, aerospace applications, and lens mirror positioning systems [3].

However, the position of USM is widely affected by the hysteresis phenomenon, and the speed-phase shift dead zone in the presence of a load torque [3]. Moreover, the resonant behavior of the motor is very sensitive to external conditions like the load torque and temperature [4]. For these reasons, accurate and precise position control of such motors is a real challenge.

Several position control strategies of USMs have been proposed. PID control has been tested in [5,6]; it is simple and easy to be implemented but it is difficult to set the parameters and to meet the performance requirements of USM. Tuning PID parameters are proposed also to overcome the shortcoming mentioned above [7]. The tuning parameters technique requires the setting of related parameters according to the USM operating state, load conditions, and temperature. Adaptive method based on reference model was proposed in [8] to compensate the dead zone. Due to the fact that fuzzy logic control is preferred when the mathematical model of a control plant is difficult to obtain, this technique was proposed in several research works to achieve superior speed and position characteristics [8–10]. It is based on the knowledge of the USM state and experimental data to make up the fuzzy inference rules. But under certain conditions, the motor parameters are variable, and the output motion can be outside the inference rules [3]. The Neural Network (NN) control is also investigated in the control system of USM [11]. It is based on the nonlinear mapping function using neurons and connection weights. With the NN better control accuracy can be obtained. However, USM behavior and parameter variation yields to the growth of the network's complexity for the NN controller which will increase the execution time and learning procedure [3]. Because the control techniques mentioned above have their advantages and disadvantages, many mixed

☆ This paper was recommended for publication by Associate Editor M. Moallem.

* Corresponding author.
E-mail addresses: mouhanned.brahim@centralesupelec.fr (M. Brahim), imen.bahri@centralesupelec.fr (I. Bahri), yves.bernard@centralesupelec.fr (Y. Bernard).

http://dx.doi.org/10.1016/j.mechatronics.2017.04.003
0957-4158/

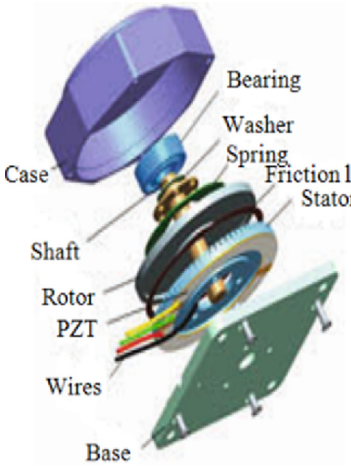

Fig. 1. Structure of rotary USM [2].

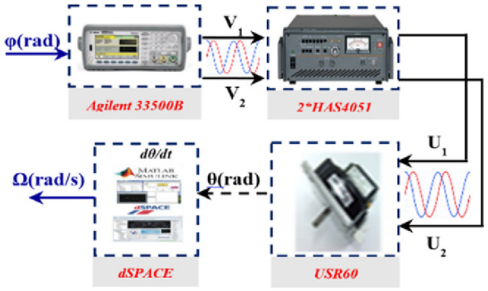

Fig. 2. Block diagram of the open loop experimental setup.

controllers have been developed, such as fuzzy neural network [12], fuzzy PID [13], NN PID [14], and Particle Swarm Optimization (PSO) combined with PID [7]. The combined controllers have shown better performances, but the implementation difficulty for engineering applications remains their main limitation.

In this paper, authors propose two robust position controllers based on continuous-time H-infinity and discrete- time RST for the TWUM (USR60). While the dynamic behavior of the USM is highly sensitive to external conditions (temperature, load), and the motor parameters are time varying. The main contribution of the proposed system is providing precise positioning without additional compensation system of the nonlinearity factors. The robustness of the presented method is proved firstly in cases of; motor parameters variation due to the nonlinear behavior around the resonance frequency, and load variation (dead zone effect). Secondly, in case of injected electrical noises to the control signal and to the measured position data. A real time implementation and a performance comparison of the two proposed controllers are carried out. The control technique and the synthesis procedure of the two proposed controllers are respectively detailed in Sections 2 and 3. The simulation results of the proposed system are presented in Section 4. The design of a compact experimental platform, the real time implementation, and the performances validation of the proposed controllers are illustrated in Section 5.

2. Motor control techniques

The USR60 motor (Fig. 1) is supplied by two phase shifted voltages. It can be controlled via the amplitude, frequency, and phase shift of driving voltages. Open loop tests are done to illustrate the motor behavior, and to identify the motor model transfer function (TF). Since the amplitude of standing waves depend on the voltage amplitude, speed and position can be controlled through adjusting the driving voltage amplitude. From the open loop experimental tests (Fig. 3a), it can be seen that a large voltage amplitude variation (40Vrms) generates a small speed variation and so on, a reduced motor motion. The driving frequency variation method gives more flexible control range. However, there is a nonlinear relationship between the speed and frequency (Fig. 3b). Moreover, a breakdown appears when the driving frequency decreases below the mechanical resonance frequency (f_r). This breakdown is well known as the pull-out phenomenon of TWUMs [3].

The voltage phase shift (φ) can be also used to adjust the motor speed and position, and it is the only parameter that allows the inversion of motor rotation direction. This method also has the problem that the speed is not nicely linear with the voltage phase shift. Moreover, there is a dead zone around zero value of phase shift when load torque (T_L) is added (Fig. 3c). Therefore, the phase shift is more suitable for a position control than a speed control. Regarding the intended use of the USM in robotic applications and the obligation of precision and bidirectional operation mode, φ is chosen as the position control parameter in this paper. For these purposes, a simplified TF between φ and the angular motor position (θ) must be identified to be used for the synthesis of the position controllers. The topology of the open loop setup for the experimental TF identification is shown in Fig. 2.

A step change of the voltage phase shift (φ) is applied at the input of the function generator (Agilent3350B), two phase shifted voltages are then generated and amplified. The corresponding position variation (θ) is measured via the rotary position encoder. The motor velocity (Ω) is then derived as illustrated in Fig. 5. The TF between φ and Ω is estimated to a first order system using the Matlab identification toolbox. The TF between φ and θ is then deduced as a second order TF [8]:

$$\frac{\theta(s)}{\varphi(s)} = \frac{k_m}{s(1+\tau_m s)} \tag{1}$$

where the gain constant k_m and the time constant τ_m are respectively equal to 10.25 and 3.5 ms.

As mentioned above, the dynamic behavior of the TWUM is nonlinear especially around the mechanical resonance frequency. Moreover, the motor output characteristics (speed/position, torque) are very sensitive to the operation conditions. Therefore, the identified TF parameters are uncertain and depending on the nonlinearity factors and driving parameters. For example the gain and time constants (k_m,τ_m) are respectively equal to 6.5 (instead of 10.25) and 9.3 ms (instead of 3.5 ms) when the motor operates at a frequency of 35 kHz. Moreover, the addition of load torque affects the motor speed and the position accuracy due to the dead zone effect (Fig. 3c). The motor resonance frequency (f_r) and rotational speed depend also on the motor body temperature as shown in Fig. 4. The frequency f_r will decrease for temperature increasing and in consequence the speed at a given frequency will decrease. Therefore, the motor heating will affect the TF parameters, where the time constant (τ_m) reaches 6 ms for an operation temperature about 45 °C. That's why we rely on the robustness of the proposed controllers to overcome the model uncertainty problems and to ensure high precision levels at any operating temperature (< 55 °C) or under any loads (up to1N.m). Adaptive controllers with on-line parameters adaptation using the fuzzy logic and neural network methods are often used to compensate the motor parameters variation and the nonlinear behavior [7–15]. However, it is at the expense of the experimental implementation simplicity and the time execution.

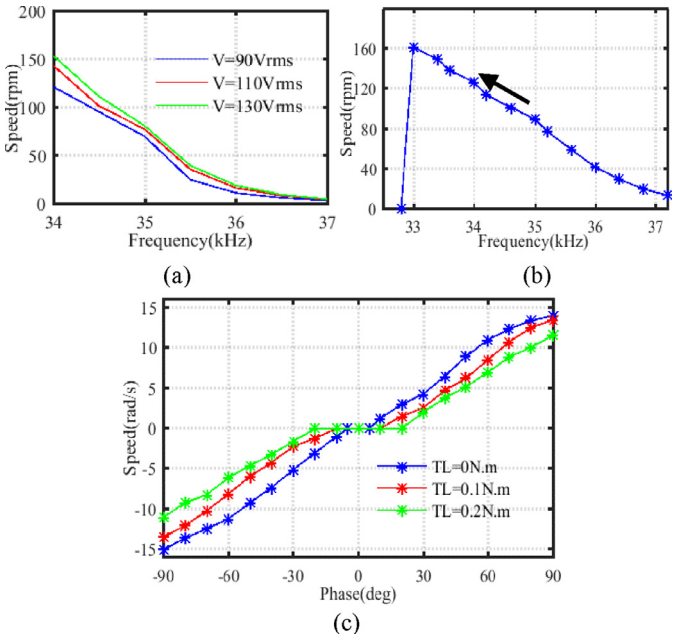

Fig. 3. Experimental speed variation as function of: (a) voltage amplitude, (b) frequency, (c) phase shift.

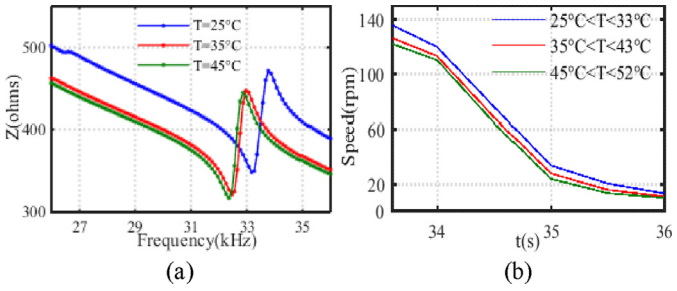

Fig. 4. Motor temperature effect on: (a) Mechanical resonance frequency, (b) motor speed.

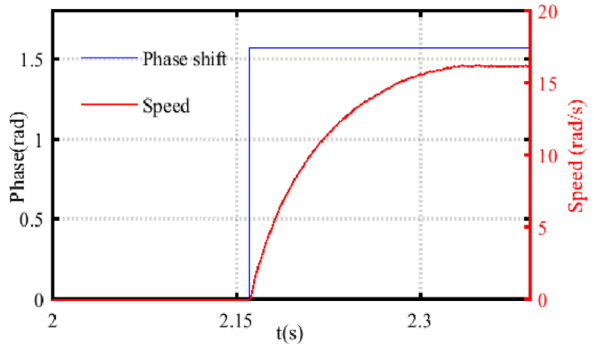

Fig. 5. Open loop speed response for $\pi/2$ phase shift step.

3. Position controllers synthesis

3.1. H-infinity controller

It is well known from robust control theory that any block diagram can be rearranged into the standard form shown in Fig. 5. The transfer matrix of a generalized system (Fig. 6) can be written as [16]:

$$\begin{pmatrix} e(s) \\ y(s) \end{pmatrix} = P(s) \begin{pmatrix} w(s) \\ u(s) \end{pmatrix} = \begin{pmatrix} P_{ew}(s) P_{eu}(s) \\ P_{yw}(s) P_{yu}(s) \end{pmatrix} \begin{pmatrix} w(s) \\ u(s) \end{pmatrix} \tag{2}$$

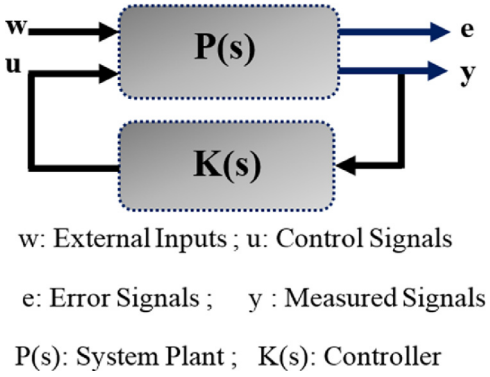

Fig. 6. Description of generalized plant.

where e, y, w, u are the inputs/outputs of the generalized plant defined in Fig. 6, and P is a state-space realization of the generalized plant.

The lower Linear Fraction Transformation (LFT) between w and e is then [16]:

$$e(s) = F_l(P(s), K(s)) w(s) \tag{3}$$

$$F_l(P(s), K(s)) = P_{ew}(s) + P_{eu}(s) K(s) (I - P_{yu}(s) K(s))^{-1} P_{yw}(s) \tag{4}$$

The synthesis of H_∞ controller consists of finding a state feedback controller K(s) that should in any case internally stabilize the closed loop system, and guarantee that the H_∞ norm satisfies the following inequality [16]:

$$\| F_1(P(s), K(s)) \|_\infty < \gamma \tag{5}$$

There are many approaches for solving the H_∞ control problem. The resolution based on Riccati equations [16] will be used in this study. In Fig. 6a, the motor plant is represented by G(s), K(s) is the controller, b is an additional disturbance, r and y are respectively the reference and measured positions. The system transfer matrix can be written as:

$$\begin{pmatrix} \varepsilon \\ u \end{pmatrix} = \begin{pmatrix} K & SG \\ KS & KSG \end{pmatrix} \begin{pmatrix} r \\ b \end{pmatrix}; \; S = \frac{1}{(1 + KG)} \tag{6}$$

where S is the sensitivity function and it can be defined as the transfer function between the reference signal r and the tracking error ε. In (6), as will be done in most of the following, the Laplace term "s" will be omitted for the sake of simplicity. The controller K (s) must satisfy the following inequality [16]

$$\left\| \begin{matrix} K & SG \\ KS & KSG \end{matrix} \right\|_\infty < \gamma \tag{7}$$

To satisfy (7) and to demonstrate the robustness of the controller, supplementary degrees of freedom should be added to the system presented in Fig. 6a. Therefore, weighting filters (W_i) are widely introduced [18] as shown in Fig. 4b. The weighting filter performances are generally derived based on frequency domain specifications. The advantage of using the topology shown in Fig. 6b instead of Fig. 6a is that the system response frequency will be fixed by the filter behaviors. The desired performances of the closed loop system will then be fixed via the filter parameters depending on the frequency operation range. The transfer matrix of the system presented on Fig. 6b will be then:

$$\begin{pmatrix} e_1 \\ e_2 \end{pmatrix} = \begin{pmatrix} W_1 S & W_1 SGW_3 \\ W_2 KS & W_2 KSGW_3 \end{pmatrix} \begin{pmatrix} r \\ d \end{pmatrix} \tag{8}$$

The controller K(s) will now satisfy:

$$\left\| \begin{matrix} W_1 S & W_1 SGW_3 \\ W_2 KS & W_2 KSGW_3 \end{matrix} \right\|_\infty < \gamma \tag{9}$$

If (9) is satisfied, the following inequalities will therefore be satisfied:

$$|S(j\omega)| < \frac{\gamma}{|W_1(j\omega)|} \tag{10}$$

$$|S(j\omega)G(j\omega)| < \frac{\gamma}{|W_1(j\omega)W_3(j\omega)|} \tag{11}$$

$$|K(j\omega)S(j\omega)| < \frac{\gamma}{|W_2(j\omega)|} \tag{12}$$

$$|K(j\omega)S(j\omega)G(j\omega)| < \frac{\gamma}{|W_2(j\omega)W_3(j\omega)|} \tag{13}$$

For the USR60 plant, the closed loop performances are fixed as:

- Time response: <10 ms
- Stability margin: $\Delta G > 10$ dB, $\Delta\varphi > 45$ deg
- Static error: $<0.1\%$

The weighting filter parameters will be then determined to satisfy the performances listed above. The expression of W_i can be written as function of frequency domain specification [17]:

$$W_i = \frac{s/M + \omega_0}{s + A\omega_0} \tag{14}$$

where ω_0 is the closed loop bandwidth, A is the minimum steady state error, and M is the high frequency amplification gain.

3.1.1. Choice of W_1

The transfer $1/W_1$ should have a low gain at low frequency to reduce the static error while the filter cut-off frequency can be interpreted as the minimal system bandwidth. For a gain of 0.01 at low frequency, W_1 is given by:

$$W_1 = \frac{(s+510)}{1.42(s+503)}$$

3.1.2. Choice of W_2

The most important parameter of W_2 is the cutoff frequency that will limit the maximum system bandwidth to avoid very fast system response and therefore high control signal values. This frequency should be much higher than the system bandwidth.

$$W_2 = \frac{(s+510)}{0.1\left(s+5.10^5\right)}$$

3.1.3. Choice of W_3

As shown in Fig. 6b, W_3 is used to filter control signal disturbance. W_3 is mostly chosen as a low constant and can be adjusted as function of disturbance rejection results.

$$W_3 = 0.1$$

Based on the filter parameters, the optimal controller and gamma constant can be found using the MATLAB function "hinfsyn". Otherwise, the obtained fourth order controller contains zeros and poles outside the system operation frequency range. The useless zeros and poles can be reduced via the "reduce" MATLAB function. Finally, an optimal gamma value and a second order controller are obtained:

$$K(s) = \frac{3.8.10^5 s + 1.12.10^8}{s^2 + 2.6.10^3 s + 3.3.10^6} \quad ; \gamma = 1.05$$

As can be seen, that the desired performances of the closed loop can be easily introduced in the frequency domain via the H_∞ control principle with the minimum controller degree. The robustness of this controller is also ensured and will be confirmed later by simulation and experimental results.

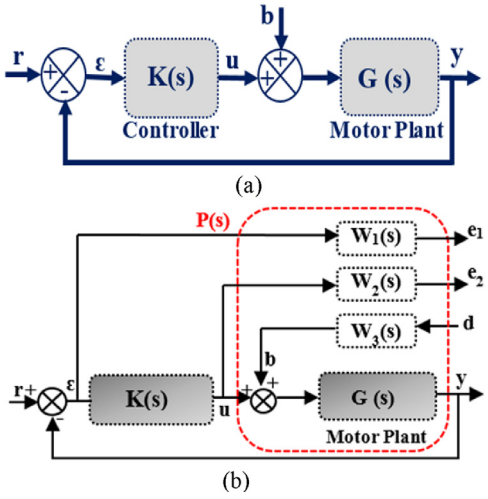

Fig. 7. (a) Closed loop system configuration, (b) With weighting filters.

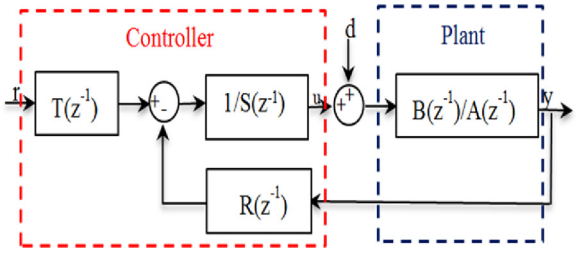

Fig. 8. Discrete time system controlled by RST regulator.

3.2. RST controller

RST control consists of a discrete pole placement method based on the resolution of Diophantine equations [19]. As shown in Fig. 7, this controller is composed by three discrete polynomials ($R(z^{-1})$, $S(z^{-1})$, and $T(z^{-1})$). The block $B(z^{-1})/A(z^{-1})$ is the discrete time open loop transfer function of USR60, d represents the disturbance, u is the control signal, and r and y are respectively the reference and measured position.

$$\begin{aligned} R(z^{-1}) &= r_0 + r_1 z^{-1} + ... + r_n z^{-n} \\ S(z^{-1}) &= s_0 + s_1 z^{-1} + ... + s_m z^{-m} \\ T(z^{-1}) &= t_0 + t_1 z^{-1} + ... + t_i z^{-i} \end{aligned} \tag{15}$$

The closed loop transfer function and the control signal are respectively given by:

$$Y(z^{-1}) = \frac{B(z^{-1})T(z^{-1})}{A(z^{-1})S(z^{-1}) + B(z^{-1})R(z^{-1})} r(z^{-1}) + \frac{S(z^{-1})}{A(z^{-1})S(z^{-1}) + B(z^{-1})R(z^{-1})} d(z^{-1}) \tag{16}$$

$$U(z^{-1}) = \frac{T(z^{-1})}{S(z^{-1})} r(z^{-1}) - \frac{R(z^{-1})}{S(z^{-1})} Y(z^{-1}) \tag{17}$$

As seen in (16), $T(z^{-1})$ appears only in the numerator giving the supplementary degrees of freedom to this controller and can be easily used to improve the tracking performances. The polynomials $R(z^{-1})$ and $S(z^{-1})$ are determined by robust pole placement strategy and will be solutions of the Diophantine equation [19]:

$$D(z^{-1}) = A(z^{-1})S(z^{-1}) + B(z^{-1})R(z^{-1}) \tag{18}$$

The polynomial $D(z^{-1})$ contains the desired poles of the closed loop system and can be written as the following:

$$D(z^{-1}) = (1 - p_1 z^{-1})(1 - p_2 z^{-2})...(1 - p_j z^{-j}) \tag{19}$$

where P_j are the desired poles of the closed loop system.

The three polynomials R, S, and T must be chosen so that the closed loop transfer function of the actual system will be equal to a reference model (H_m) fixed in advance as a function of the desired closed loop performances:

$$H_m(z^{-1}) = \frac{B_m(z^{-1})}{A_m(z^{-1})} = \frac{y(z^{-1})}{r(z^{-1})} \tag{20}$$

To ensure the system stability, the denominator A_m must only contain poles inside the unit circle. The numerator B_m will have as a factor the plant pure delay and the zeros that remain uncompensated [19]. Thus B_m can be written as:

$$B_m(z^{-1}) = B^-(z^{-1})B'_m(z^{-1}) \tag{21}$$

In order to ensure unity gain in the steady state ($H_m(1)=1$), the polynomial T will be given by [20]:

$$T(z^{-1}) = A_0 B'_m(z^{-1}) \tag{22}$$

where A_0 is a filter polynomial that will be used to adjust the static error.

In the case of a sinewave reference signal, in order to cancel the steady state error, auxilliary Diophantine equation must be solved [19]. The transfer function from the reference (r) to the true error signal (ε=y−r) between reference and measured position is given by:

$$\frac{\varepsilon(z^{-1})}{r(z^{-1})} = 1 - \frac{y(z^{-1})}{r(z^{-1})} = 1 - H_m(z^{-1}) \tag{23}$$

and its magnitude is given by

$$\left|\frac{\varepsilon}{r}\right|_{z=e^{j\omega T_s}} = \left|\frac{A_m - B_m}{A_m}\right|_{z=e^{j\omega T_s}} \tag{24}$$

where T_s is the sampling period of the plant.

To cancel the error at a given angular frequency (ω_0), it is necessary to introduce a transmission zero into this transfer function at that frequency. If we assume that a complex conjugate pair of zeros will be introduced, then $(1\text{-}e^{j\omega_0 T_s}z^{-1})\,(1\text{-}e^{-j\omega_0 T_s}z^{-1})$ must divide A_m-B_m. This condition can be written as [19]:

$$A_m - B_m = \left(1 - e^{j\omega_0 T_s}z^{-1}\right)\left(1 - e^{-j\omega_0 T_s}z^{-1}\right)L(z^{-1})$$

$$= (1 - 2\cos(\omega_0 T_s)z^{-1} + z^{-2})L(z^{-1}) \tag{25}$$

Therefore, the auxiliary Diophantine equation that must be solved is:

$$A_m = (1 - 2\cos(\omega_0 T_s)z^{-1} + z^{-2})L(z^{-1}) + B^- B'_m \tag{26}$$

To illusrate the synthesis aproach for the USR60 motor, the continuos time model of the motor is sampled with a samplig period Ts= 0.1 ms:

$$G(z^{-1}) = \frac{B(z^{-1})}{A(z^{-1})} = \frac{10^{-5}(1.43z^{-2} + 1.45z^{-1})}{0.97z^{-2} - 1.97z^{-1} + 1}$$

This plant is designed to be controlled so that the closed loop has a second order type with a damping factor of 0.7 and a bandwidth of 500 rad/s. Thus a discrete charachteristic polynomial is obtained:

$$A_m = 1 - 1.92z^{-1} + 0.932z^{-2}$$

By the resolution of the primary Diophantine Eq. (18), the polynomials $S(z^{-1})$ and $R(z^{-1})$ can be obtained:

$$S(z^{-1}) = 1 + 0.02z^{-1};\ \ R(z^{-1}) = 1.47 - 1.38z^{-1}$$

For a sinusoidal reference signal with $\omega_0 = 10$ rad/s, the auxiliary Diophantine Eq. (26) is:

$$(1 - 2z^{-1} + z^{-2})L(z^{-1}) + 10^{-5}(1.43z^{-2} + 1.45z^{-1})B'_m$$
$$= 1 - 1.92z^{-1} + 0.932z^{-2}$$

Table 1
Controller performances.

	H-infinity	RST
Phase margin(deg)	70.9	61.5
Gain margin(dB)	24.2	33.4
Response time(ms)	6	10

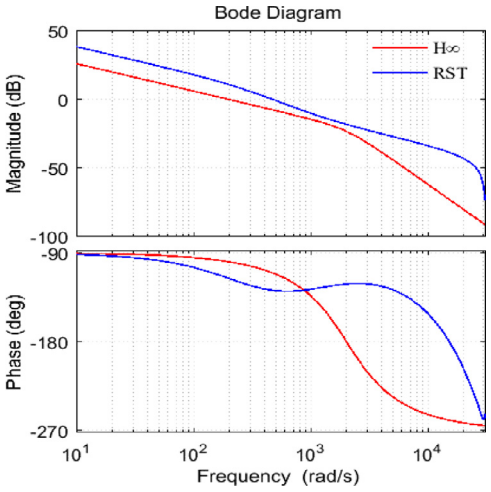

Fig. 9. Bode diagrams.

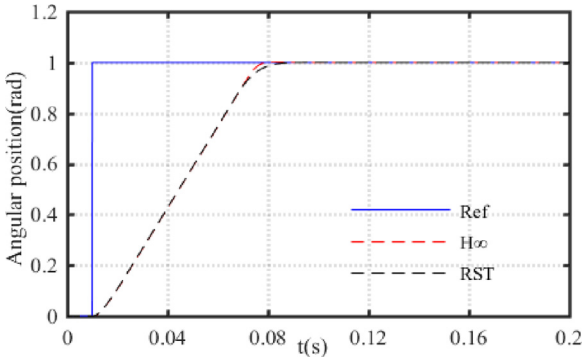

Fig. 10. Comparison of step responses.

Therefore, the polynomials $L(z^{-1})$ and $T(z^{-1})$ are deduced:

$$L(z^{-1}) = 1 + 0.034z^{-1};\ \ T(z^{-1}) = 2.46 - 2.38z^{-1}$$

The discrete time synthesis of the RST controller minimizes the delays introduced by the conversion stages of a continuous regulator. The robust pole placement method is efficient for the tracking of polynomial reference signals. Moreover, the third degree of freedom which is the polynomials T can be easily used to ameliorate the tracking performances as will be confirmed after.

4. Simulation results

In this section, the simulation results of the closed loop system are presented to verify the controller performances. The stability, time response, precision, and robustness are also evaluated and compared. The stability of the closed loop system is guaranteed with the two proposed controllers as indicated in Table 1 and Fig. 9. The phase shift (φ) between the two driven voltages of TWUM must be limited between $+/-\pi/2$ for practical use, because outside of this range the motor behavior will be highly nonlinear [8]. The two proposed controllers show quick response without overshoot as illustrated in Fig. 10. The time analysis of the closed

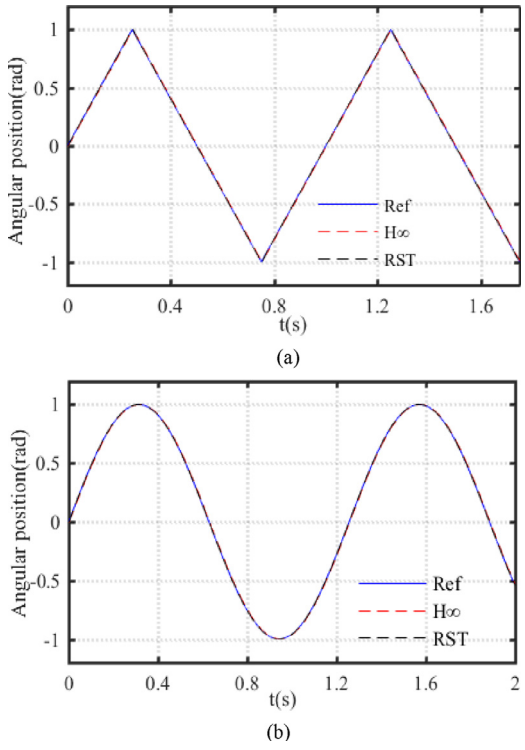

Fig. 11. Comparison of position responses: (a) Triangular motion, (b) Sine wave motion.

loop system controlled by H_∞ and RST for different position trajectories is shown in Fig. 11. The two proposed controllers show high precision levels with zero steady state error and no overshoot. The motor speed depends on the driving frequency, motor temperature, and load torque. Therefore, the identified motor TF parameters (k_m, τ_m) will change if the motor operation conditions change. Thus, the robustness of the position controllers in the case of motor parameter variation is evaluated. The two presented controllers are compared also to a PID controller to confirm the advantage of the proposed methods. The PID parameters are determined based in the motor TF (1) and tuned by trial –and-error through intensive tests. The resulting PID parameters are finally; $K_{p=}5$, $K_i = 0.1$, and $K_d = 1.15$. Fig. 12 presents the position responses respectively in case of gain constant (k_m) decreases by a ratio of 51% (5 instead of 10.25), and in case of time constant (τ_m) increases by a ratio of 71.5% (6 ms instead of 3.5 ms). The simulation results show that the response of the three designed controllers is not much affected by the gain constant variation (Fig. 12a). Whereas, the time constant variation generates an overshoot of respectively 0.5%, 0.9%, and 3% for the RST, H_∞ and PID controllers as illustrated in Fig. 12b. To simulate the eventual electrical noises in the generated control signal (φ) or in the measured position (θ), external Gaussian random noises are injected to the closed loop system to examine the perturbation rejection capability of the position controllers. The difference between the three controllers in term of control signal noises rejection can be deduced from the amount of the output position distortion in Fig. 13a. For an injected control signal noises of +/−0.1 rad, the output position distortion is of +/−0.001 rad for the RST and H_∞ and of +/−0.005 rad for the PID controller. The measured position is perturbed, by a high frequency signal noises (+/−0.1 rad/10 kHz) equivalent to the noises that can be generated by the position sensing and conversion stage. Fig. 13b shows that the motor position is much affected by the measurement noises. In this case, as illustrated in Fig. 13b, the robustness of the H_∞ can be easily distinguished compared to the rest of controllers. In fact

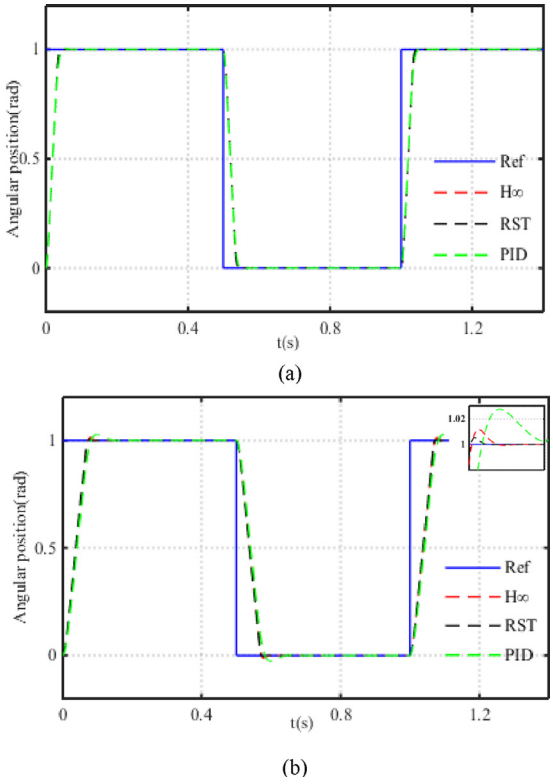

Fig. 12. Controller performances under motor parameters variation: (a) $k_m = 5$, (b) $\tau_m = 6$ ms.

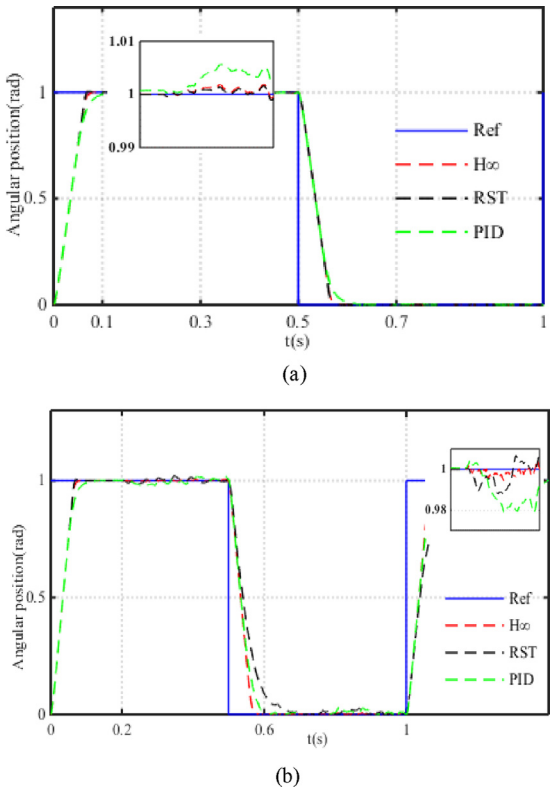

Fig. 13. Comparison of position step responses under: (a) Control signal noises (t= 0.2 s), (b) measurement noises (t= 0.2 s).

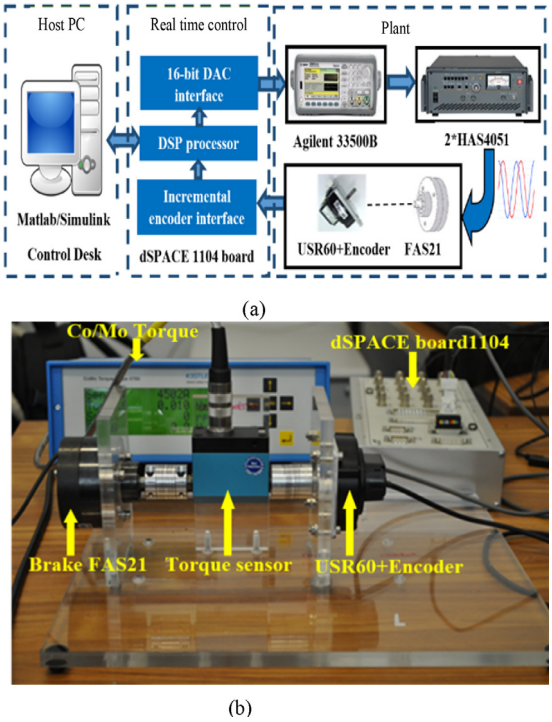

Fig. 14. (a) Block diagram of experimental setup, (b) Experimental platform.

with the H_∞ controller, we keeps a maximum position distortion of +/−0.007 rad for a step position of 1 rad. Moreover, the time responses of the positioning system based on PID and RST controllers is affected by these noises, and it is not the case with the H_∞ controller.

5. Experimental validation

5.1. Experimental platform description

To implement the described control methods, a compact system is designed as shown in Fig. 14b. The experimental platform consists of rotary TWUM from Shinsei.Co (USR60-E3T) with a coupled optical encoder. The load torque is generated using a powder brake (FAS21) with a rated torque of 2 N.m. The torque is measured and conditioned via a mini-smart torque sensor with a control/monitoring board from Kistler. A dSpace controller board from dSpace (DS1104) is used for the closed loop real time control. The DS1104 obtains the position data from the encoder, and one of the presented control methods is executed. The control signal (φ) is then calculated and sent to a dual channels waveform generator. Two phase shifted sinusoidal voltages are generated and connected to two power amplifiers (HSA4051) to drive the ultrasonic motor (Fig. 14a). The motor tests show that the mechanical resonance frequency and consequently the motor speed changes as functions of the motor temperature. Because of this, the closed loop tests are done with a driving frequencies higher than f_r to avoid the instability around the resonance frequency.

5.2. H-infinity test results

The H-infinity controller is tested with different position trajectories, variable driving frequencies, and in the presence of load torque. In Fig. 15, the control method is tested with a rotor velocity of 10 rpm (f_r= 36 kHz) and without load. As can be seen, there are no overshoot with a static error of 0.09 (0.1% which

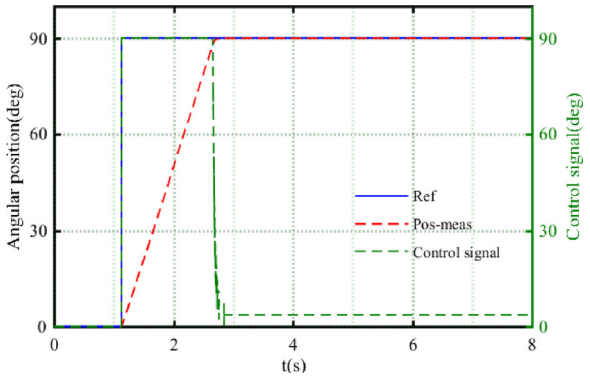

Fig. 15. Step response of H_∞ position controller.

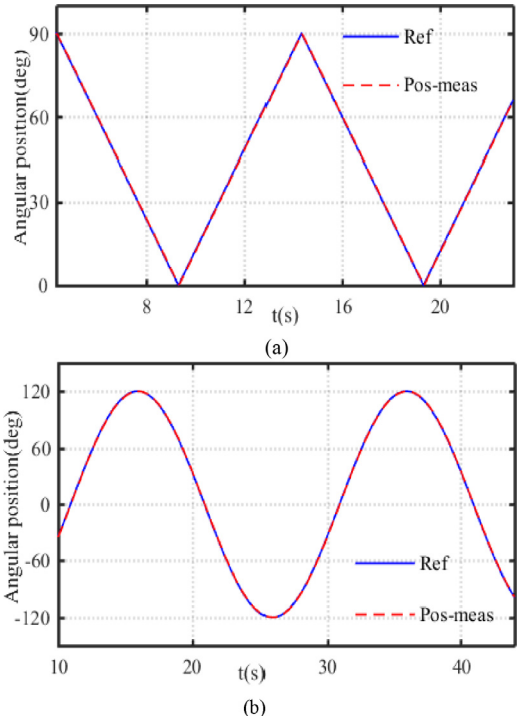

Fig. 16. H_∞ response for variable position trajectory: (a) triangular motion, (b) Sine-wave motion.

is the maximum resolution of the encoder). The tracking performances of different position trajectories are tested at the driving frequency 35 kHz (30 rpm) showing similar results in terms of precision and response time (Fig. 16). When a load torque is applied, a dead zone appears at the phase-speed characteristic (Fig. 3c). A dead zone compensation system is almost used in addition to the position controller [8,22,23]. In this paper, the challenge is to validate the precision and the robustness of the positioning system in the presence of dead zone and without compensation system. The H_∞ closed loop system keeps a high precision level in case of loaded motor, where the steady state error is of 0.36 for a position step of 90 when a load torque of 0.35 N.m is applied (Fig. 17). It should be mentioned also that for the case of 0.35 N.m the dead zone reaches +/−30 .

Due to the friction system between the stator and rotor of the TWUM, the motor temperature will increase if no cooling system is used. The motor parameters and performances of TWUM are temperature-depending [21,24,25]. In order to validate the performances of the proposed system under any motor temperature (up to 55 °C), the H_∞ is tested under different motor temperatures

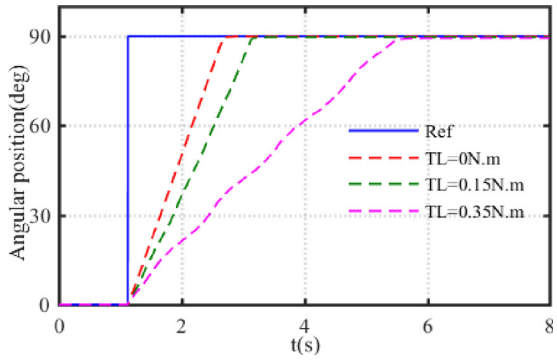

Fig. 17. Step response of H_∞ position controller with load torques.

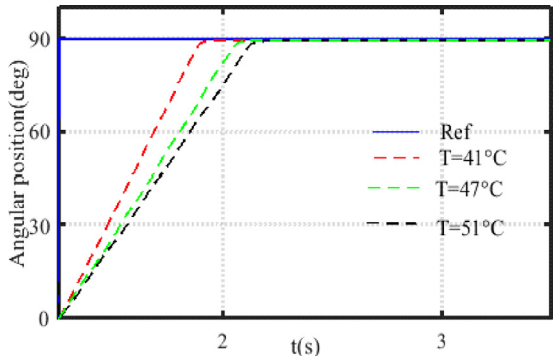

Fig. 18. . H_∞ response under different temperatures.

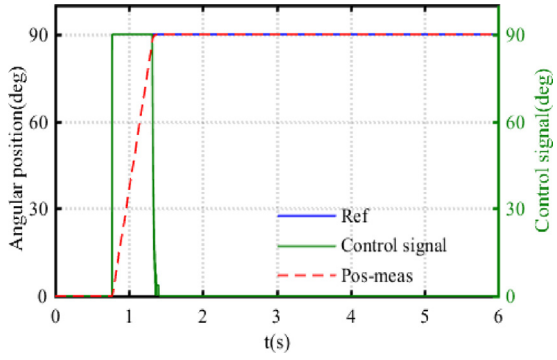

Fig. 19. Step response of RST position controller.

(Fig. 18). The precision is always guaranteed under temperature increasing. As shown in Fig. 18 for an operation temperature of 51 °C, the maximum static error is of 0.4 for a rotation of 90 .

5.3. RST test results

The RST position controller is synthesized in discrete time with a sampling period of 0.1 ms. The position step response and the control signal of the RST controller with a driving frequency of 35 kHz are presented in Fig. 19. Similar to the other controller, there is no overshoot of the step response with a precision of 0.1%.

The RST controller with auxiliary Diophantine equation shows high precision levels for polynomials position reference and especially for the sine-wave trajectory (Fig. 20), where the reference signal frequency is taken into account in the synthesis procedure. The loaded motor tests show that the static error increases significantly. One solution to ameliorate the precision is to use the polynomial $T(z^{-1})$. For the loaded motor tests the filter A_0 (27) is taken slightly higher than one. The test with modified polynomials gives a static error between 0.1% and 1% (Fig. 21).

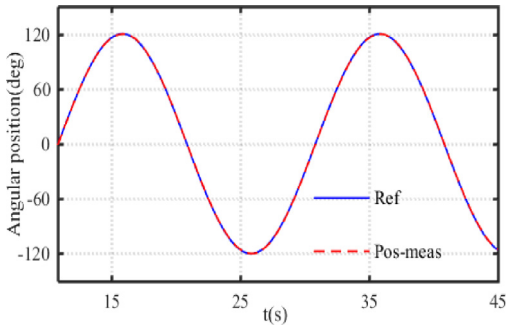

Fig. 20. RST response for sine-wave motion.

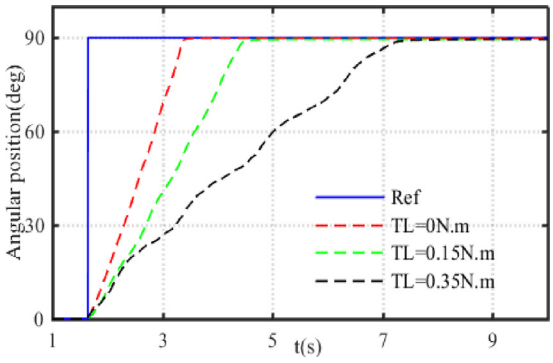

Fig. 21. RST step response with load torques.

Table 2
Static error as function of load torques.

TL(N.m)	H-infinity	RST	PID
0.1	0.1%	0.3%	0.4%
0.3	0.25%	0.6%	1%
0.5	0.4%	1%	1.65%

5.4. Comparison of controller performances

In this section a comparative study between the H-infinity, RST, and a conventional PID controllers will be presented. The comparison criteria are the precision and time response, load torque (dead-zone) sensitivity, adaptation with polynomial reference signals, and the rejection of control signal or measurement disturbances. The proposed controllers show good performances in terms of time response and precision in case of no-load tests and without motor heating. However, when load torque is added, the H_∞ controller gives higher precision levels and faster response times as shown in Fig. 22 for load torques of 0.1 N.m and 0.2 N.m. The degradation of the precision levels is explained by the dead zone around zero phase values in the speed-phase shift characteristics with load torques (Fig. 2c). The robustness of the H_∞ controller can be easily distinguished in these cases, where the controller gives a static error less than 0.1 in case of 90 rotation under 0.2 N.m. The resulting static error ratios of the three controllers in the case of loaded motor step response (90) are summarized in Table 2. From this table, it is clear that the very high precision levels can be achieved with the H_∞ controller. Fig. 23 shows the comparison test results for sinus position response (120) with a load torque of 0.2 N.m, giving a maximum static error of 0.65% (0.8) for H_∞, 1% (1.2) for RST, and 1.8% (2.2) for PID controller. The disturbances rejection capability of the three proposed controllers is also compared. Additional Gaussian random noises are injected to the closed loop system as a kind of system disturbances. Firstly, a high frequency noises is injected to the measured position data (encoder output)

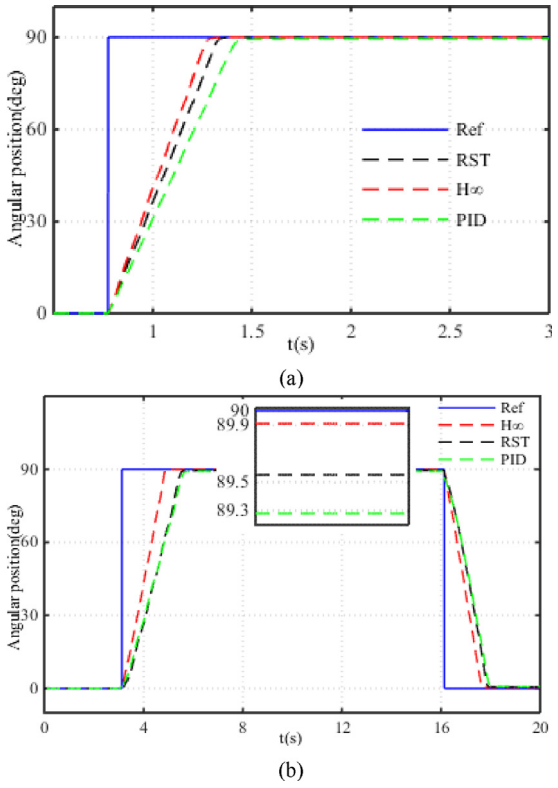

Fig. 22. Comparison of H_∞, RST and PID step position responses for loaded motor: (a) 0.1 N.m, (b) 0.2 N.m.

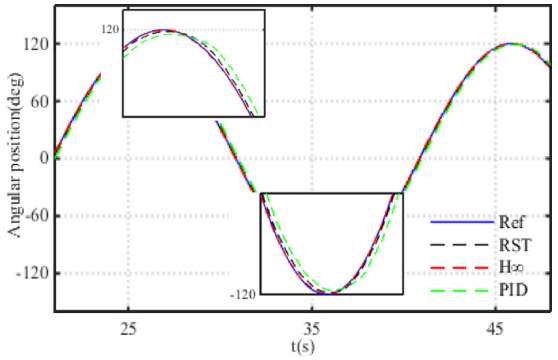

Fig. 23. Comparison of H_∞, RST and PID sinus position responses for loaded motor.

to anticipate the noises that can be generated by the position sensing system. Secondly the control signal (φ) is perturbed by injecting additional oscillations (Fig. 24a). The proposed positioning system show high rejection capability of the control signal distortion as shown in Fig. 24a. Where for an injected perturbation of $+/-5$ of the control signal, the maximum position distortion is of 0.3. However, when the measured position is perturbed by high frequency signal (10 kHz) and an amplitude of $+/-5$, the robust H_∞ position controller shows much better rejection capability than the RST and PID controllers as illustrated in Fig. 24b. In the zoomed area of this figure, the resulting static error is respectively of 0.3, 1 and 1.6 for the H_∞, RST, and PID controllers.

6. Discussion and conclusion

In this paper, the authors have successfully designed and implemented two robust position controllers of rotary TWUM (USR60). The proposed control methods provide precise and robust motion

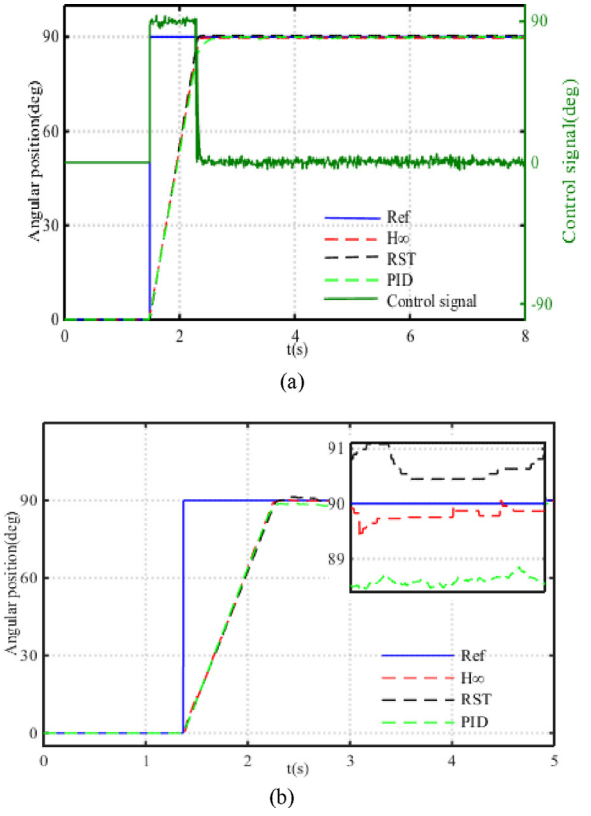

Fig. 24. Comparison of position step responses under: (a) Control signal noises, (b) measurement noises.

control despite the uncertain and nonlinear motor model, and the motor resonance behavior variation.

As a first step the desired closed loop performances are fixed and the design procedure of H_∞ and RST controllers was detailed. Then, the obtained controller parameters are validated with Matlab/Simulink simulations. The proposed controllers have been implemented on a custom designed experimental platform with real time control. The obtained results confirm the precision and robustness of the presented position controllers. The performances of the closed loop system with loaded motor, under different temperatures, and in case of external injected noises have been evaluated and confirmed. In case of loaded motor, with the H_∞ controller a high precision level is achieved without additional compensation system of the dead zone. A comparative study between the H_∞, RST, and conventional PID controllers is also proposed to confirm the superiority of the proposed method. The perturbation rejection capability tests show that the H-infinity controller is more robust than the rest of controllers mainly in the case of position measurement noises.

References

[1] Sashida TKenjo. An introduction to ultrasonic motors. New York: Oxford University Press; 1993.
[2] Maas J, Schulte T, Fröhleke N. Model-based control for ultrasonic motors. IEEE/ASME Trans Mechatronics 2000;5(2):165–80.
[3] Zhao Ch. Ultrasonic motors: technologies and applications. Science Press Beijing; 2011.
[4] Mashimo T, Terashima K. Experimental verification of elliptical motion model in traveling wave ultrasonic motors. IEEE/ASME Trans Mechatronics 2015;20(6):2699–707.
[5] Gencer A. A new speed/position control technique for travelling wave ultrasonic motor under different load conditions. PEMC 2014:65–70.
[6] Li H, Sun Z, Huang W. Control of multiple ultrasonic motors with robust parameter design. IEEE Ultrason Symp 2008:1827–30.
[7] Tanaka K, Djoewahir A, Nakashima S. Adaptive PSO-based self-tuning PID controller for ultrasonic motor. Int J Innov Comput Inf Control 2013;9(10):3903–14.

[8] Senjyu T, Kashiwagi T, Uezato K. Position control of ultrasonic motors using MRAC and dead-zone compensation with fuzzy inference. IEEE Trans Power Electron 2002;17(2):265–72.
[9] FBazrafshan BRasti, Mojallali H. Fuzzy modeling and position control of a traveling wave ultrasonic motor. ICCAE 2010:457–61.
[10] Bal G, Bekiroglu E, Demibras S, Colak I. Fuzzy logic based DSP controlled servo position control for ultrasonic motor. J Energy Convers Manage 2004;45:3139–53.
[11] Ahmadi M, Mojallali H, Fotovvati MH. Predictive control of traveling wave ultrasonic motors using neural network. PEDSTC 2011:256–61.
[12] Lin F-J, Wai R-J, Lin H. Adaptive fuzzy-neural-network controller for ultrasonic motor drive using LLCC resonant technique. IEEE Trans Ultrason Ferroelectr Freq Control 1999;46(3):715–27.
[13] shi J, Zhao J, Cao Z, Liang Y, Yuan L, Sun B. Self-tuning fuzzy speed controller of travelling wave ultrasonic motor. Int J Smart Sensing Intell Syst 2014;7(1):301–20.
[14] Mu Sh, Tanaka K, Nakashima Sh. Intelligent control of USM using a modified NN with PSO. IEEE GCCE 2015:507–10.
[15] Bal G, Bekiroglu E. A highly effective load adaptive servo drive system for traveling wave ultrasonic motor. IEEE Trans Power Electron 2005;20(5):1143–9.
[16] Skogestad S, Postlethwaite I. Multivariable feedback control: analysis and design. New York, NY, USA: Wiley; 2007.
[17] Ortega MG, Vargas M, No FC, Rubio FR. Improved design of the weighting matrices for the S/KS/T mixed sensitivity problem— application to a multivariable thermodynamic system. IEEE Trans Control Syst Technol 2006;14(1):82–90.
[18] Beaven RW, Wright MT, Seaward DR. Weighting function selection in the H_∞ design process. Control Eng Pract 1996;4(5):625–33.
[19] Ostertag E, Godoy E. RST-controller design for sinewave references by means of an auxiliary diophantine equation. In: Proc. IEEE conf. decision and control; 2005. p. 6905–10.
[20] Brahim M, Bahri I, Bernard Y. Modeling and RST position controller of rotary traveling wave ultrasonic motor. IEEE ICSPC 2015:22–7.
[21] Tavallaei M-Ali, Atashzar S-Farokh, Drangova M. Robust motion control of ultrasonic motors under temperature disturbance. IEEE Trans Ind Electron 2016;63(4):2360–8.
[22] Chen T-Ch, L B. Precise motion control with dead zone estimation and compensation using GRNN for TWUSM drive system. Expert Syst Appl 2009;36(8):10931–41.
[23] Huafeng L, Chenglin G. Quick and precise position control of ultrasonic motors using adaptive controller with dead zone compensation. J Electr Eng 2002;53(7-8):197–201.
[24] J Hu Lu, Zhao C. Analyses of the temperature field of traveling-wave rotary ultrasonic motors. IEEE Trans Ultrason Ferroelectr Freq Control 2011;58(12):2708–19.
[25] Li SY, Ou WC, Yang M, Guo C, Lu CY, Hu JH. Temperature evaluation of traveling-wave ultrasonic motor considering interaction between temperature rise and motor parameters. Ultrasonics 2015;57:159–66.

Mouhanned Brahim (M.Brahim): PhD student with the Group of electrical engineering of Paris (GeePs), University of Paris Sud, 11 rue Joliot Curie 91,192 Gif sur Yvette, France.

Imen Bahri (I.Bahri): Associate professor with the Group of electrical engineering of Paris (GeePs), University of Paris Sud, 11 rue Joliot Curie 91,192 Gif sur Yvette, France.

Yves Bernard (Y.Bernard): Professor with the Group of electrical engineering of Paris (GeePs), University of Paris Sud, 11 rue Joliot Curie 91,192 Gif sur Yvette, France.